Prototype Reynolds Number VIV Tests on a Full-scale Rigid Riser

Decao Yin[*]
SINTEF Ocean[†]
Trondheim, NO-7052
Norway
Email: decao.yin@sintef.no

Halvor Lie
SINTEF Ocean
Trondheim, NO-7052
Norway

Rolf J. Baarholm
STATOIL
Stjørdal, NO-7500
Norway

ABSTRACT

Slender offshore structures in deep water subjected to currents may experience vortex-induced vibrations (VIV), which can cause significant fatigue damage. Extensive experimental researches have been conducted to study the VIV in the past several decades. However, most of the experimental works have small-scale models and relatively low Reynolds number (Re) - 'subcritical' or even lower Reynolds number regime. There is a lack of full understanding the VIV in prototype Re flow regime. Applying the results with low Re to a full scale riser with prototype Re might have uncertainties due to the scaling effects. In addition, the surface roughness of the riser is also an important parameter, especially in critical Re regime, which is the case for prototype risers.

In present study, two full-scale rigid riser models with different surface roughness ratios were tested in the towing tank of MARINTEK in 2014. Stationary tests, pure cross-flow (CF) free oscillation tests and forced/controlled motion tests were carried out.

Several conclusions could be made:

1. *The drag coefficient is dependent on the Re number and surface roughness ratio.*
2. *At critical and supercritical flow regimes, the displacement amplitude ratio is less sensitive to Re than that at lower Re. The displacement amplitude ratio in subcritical flow regime is significantly larger than that in critical and supercritical flow regimes.*
3. *Two excitation regions for the 'smooth riser' and one excitation region for the 'rough riser' are identified.*

Nomenclature

A^* Peak/maximum amplitude ratio.
A_{nom} Nominal amplitude ratio.
C_D Drag coefficient.
C_e Excitation coefficient.
CF Cross-flow.
D Outer diameter of the riser model.
F_h Hydrodynamic force
F_{h0} Amplitude of harmonic hydrodynamic force
F_m Measured force in forced motion test
f_{osc} Oscillation frequency

[*]Corresponding author.
[†]Earlier MARINTEK, SINTEF Ocean from 1st January 2017 through a merger internally in the SINTEF Group.

f_v Vortex shedding frequency
$\hat{f} = (f_{osc}D)/U$ Non-dimensional oscillation frequency
IL In-line.
k/D Roughness ratio
L Length of the riser model
m^* Mass ratio
NDP Norwegian Deepwater Programme.
OQUS Optical tracking system.
PSD Power spectral density.
Re Reynolds number.
St Strouhal number.
T_n Natural period.
TrBL Transition in boundary layer.
TrS Transition around separation, laminar boundary layer.
TrSL Transition in shear layer.
TrS Transition around separation, laminar boundary layer.
U Current velocity.
$U_r = (UT_n)/D$ Reduced velocity.
VIV Vortex-induced vibrations.
Y_{disp} Displacement in y direction (CF).
Δl Distance between measurement stations.
ΔM Bending moment difference.
σ_{CF} Standard deviation of CF motion.
ν Kinematic viscosity.
ρ Density of the fluid.
φ Phase angle between CF motion and hydrodynamic force.
ζ Damping ratio.

1 Introduction

A literature review on the effects of Reynolds number ($Re = UD/\nu$) and surface roughness ratio on the VIV responses was conducted by [**?**]. The drag coefficient, maximum response amplitude, Strouhal number and excitation coefficients are strongly dependent on Re and surface roughness in the critical and post-critical flow regime, indicating that these effects should be accounted for in future VIV analysis. A 'scaling' method on the excitation coefficients was introduced to account for various Reynolds number and surface roughness.

Several studies investigated the Reynolds number effects on the peak CF amplitude ratio of a freely oscillating rigid circular cylinder [**?**] [**?**]. By studying experimental results, both studies demonstrated that the peak CF amplitude ratio depends on the Reynolds number and damping. However, mainly due to the limit of experimental setup, the Reynolds number ranges are 525 - 2600 in [?] and 500 - 33000 in [?] respectively, both are in the subcritical flow regime. In addition, the surface roughness effect on the response amplitude was not studied.

The response of flexible pipes was reviewed by [**?**]: the Reynolds number ranges from 10^3 to 2×10^5, and it was found that the response amplitude increases with an increased Reynolds number. Shell studied flexible pipe VIV model tests in [**?**], which were carried out at MARINTEK's Ocean Basin. The Reynolds number range is roughly 5×10^3 - 2.2×10^5. The Reynolds number effect on the response found by [?] was confirmed, the influence of surface roughness ratio is also mentioned in [?]. The influential parameters on the responses have similarities between a flexible pipe and a freely oscillating rigid cylinder.

There are few experimental studies on VIV at prototype Reynolds number ($> 10^5$), mainly due to the limitations of the test facilities. ExxonMobil performed full-scale Re number VIV model tests on a rigid bare riser and a riser with helical strakes, the Reynolds number ranges from 8×10^4 to more than 10^6 [**?**]. Various surface roughnesses were modelled by using sandpaper. It was found that in the critical Reynolds number regime, the VIV response amplitude and the excitation coefficient of a bare riser are sensitive to the Reynolds number and surface roughness. In DeepStar high Reynolds number experiments, combined in-line (IL) and CF VIV experiments were carried out at a Reynolds number range from 3.1×10^5 to 7.1×10^5 [**?**]. A rough cylinder was tested, the desired roughness was achieved by fitting a fibreglass sleeve outside the smooth cylinder, and covered in sand particles, the surface roughness ratio $k/D = 2.3 \times 10^{-3}$ [?]. 'Dual resonance' was observed for both subcritical smooth cylinder tests and supercritical rough cylinder tests when IL motion was allowed. Large 3^{rd} order harmonic lift force components were measured at prototype Reynolds number. Stable 'figure 8' response orbits were observed in supercritical Re tests.

To fill the knowledge gap regarding VIV at prototype Re and overcome shortage of applying results at lower Re to prototype Re, a new innovative VIV test rig was designed and built at MARINTEK to test a full-scale rigid riser model. This test rig was first used to study possible VIV suppression to improve operability of retrievable riser systems with auxiliary lines by adding riser fins; the model tests were carried out during 2011/2012 [**?**]. In MARINTEK's very first prototype Re VIV tests on a full-scale riser section [?], a distinct difference in response amplitude ratios was observed between 'critical' and 'subcritical' Re flow regimes, the largest amplitude ratio in 'critical' Re is around 60% of that in 'subcritical' Re.

Preliminary results of present study was published in [**?**].

2 Theoretical Background

A brief introduction of the governing equation of motion of a freely oscillating vertical circular cylinder in transverse direction (CF) is:

$$m\ddot{y} + c\dot{y} + ky = F_h \tag{1}$$

where m is total oscillating structural mass, c is structural damping, k is stiffness, F_h is hydrodynamic force exerted by the fluid in CF direction, in this study, the fluid is water. Due to the cylinder is vertical, there is no gravity force in in equation (**??**).

Some of the dimensionless parameters of equation (**??**):

Mass ratio

$$m^* = \frac{m}{\frac{1}{4}\pi\rho D^2 L} \tag{2}$$

Damping ratio

$$\zeta = \frac{c}{2\sqrt{k(m+m_a)}} \tag{3}$$

where m_a is the added mass.

Reduced velocity

$$U_r = \frac{UT_n}{D} \tag{4}$$

where T_n is the natural period in still water.

If the CF displacement is harmonic, it can be described by

$$y(t) = y_0 sin(\omega_{osc} t) \tag{5}$$

where $\omega_{osc} = 2\pi f_{osc}$; f_{osc} is oscillation frequency.

The hydrodynamic force is reasonably represented by

$$F_h(t) = F_{h0} sin(\omega_{osc} t + \varphi) \tag{6}$$

where φ is the phase angle between the motion and hydrodynamic force in CF direction.

For a circular cylinder undergoing forced motion, equation (**??**) becomes

$$m\ddot{y} - F_h = F_m \tag{7}$$

where F_m is measured force.

The following non-dimensional coefficients are discussed in this paper:

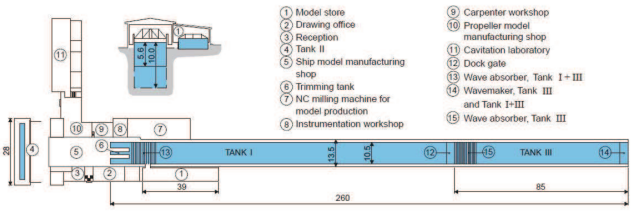

Fig. 1: Principle sketch of MARINTEK's towing tank.

The drag coefficient is defined by

$$C_D = \frac{\bar{F}_{IL}}{\frac{1}{2}\pi\rho DLU^2} \tag{8}$$

where $\bar{F}_{IL}$ is the mean force in the IL direction.

The hydrodynamic force in equation (**??**) can be decomposed into two parts: one is in phase with oscillating velocity, the other is in phase with oscillating acceleration [**?**]:

$$F_h(t) = F_{h0}sin(\varphi)cos(\omega_{osc}t) + F_{h0}cos(\varphi)sin(\omega_{osc}t) \tag{9}$$

The average fluid energy transfer rate is expressed as

$$\lim_{k\to\infty} \frac{\int_t^{t+kT} F_h(\tau)\cdot\dot{y}(\tau)d\tau}{kT} = \frac{1}{2}\omega_{osc}y_0F_{h0}sin(\varphi) \tag{10}$$

where k is the number of oscillation periods, $\dot{y}$ is oscillation velocity in CF direction.

By normalizing the hydrodynamic force component which is in phase with oscillating velocity - $F_{h0}sin(\phi)$ in equation (**??**), the dynamic excitation coefficient at oscillation frequency ω_{osc} is derived as [**?**]:

$$C_e = \frac{F_{h0}sin(\varphi)}{\frac{1}{2}\rho DLU^2} = \frac{4}{\rho DLU^2\omega_{osc}y_0}\lim_{k\to\infty}\frac{\int_t^{t+kT} F_h(\tau)\cdot\dot{y}(\tau)d\tau}{kT} \tag{11}$$

This force coefficient defines the energy transfer between fluid and cylinder for each harmonic component present in the time series. A positive value means that energy is transferred from the fluid to the cylinder, while a negative coefficient indicates energy dissipation through hydrodynamic damping. A similar approach can be used to determine an added mass coefficient, as presented in [?] [?].

3 Test Set-up

The model tests were performed in MARINTEK's towing tank, consisting of Tank I and Tank III. As shown in Fig. **??**, there is a removable dock gate between the two tanks. Tank I and Tank III can be used simultaneously or as one long tank (Tank I + Tank III) by removing a gate. In the present study, all the tests are performed in Tank I + Tank III. The water depth of Tank I is 5.6 m and 10 m for Tank III. The total length is 260 m, and it is 10.5 m wide. The towing tank is equipped with an overhead towing carriage, which can run along the tank in both directions.

During tests, a full-scale VIV test rig was hinged to the carriage. The test rig was manufactured by MARINTEK to test prototype riser models, and first used by [?]. A principle sketch of the test rig is shown in Fig. **??**. A photo with the test rig and the smooth riser model is shown in Fig. **??**.

The test rig comprises three vertical steel truss works, hinged together in a U-shape. The full-scale riser model with an outer diameter of 0.533 m was mounted onto the test rig vertically and submerged in water. Two end-plates with a diameter of 2 m were fitted at both ends of the riser model, so that the boundary effects from the water surface and bottom of the tank could be mitigated, and the flow over the test riser section was close to two dimensional.

Above the upper end-plate, the cone-shape support structure is partly submerged in water and exposed to current during tests. The submerged part is 0.9 m long, with a varying outer diameter from 0.356 m to 0.494 m. There might be extra

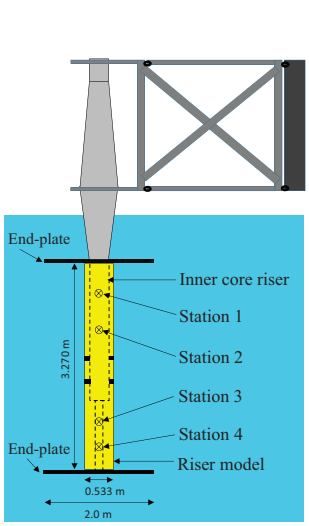

(a) Side view.

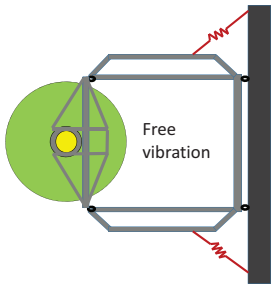

(b) Top view of free vibration set-up.

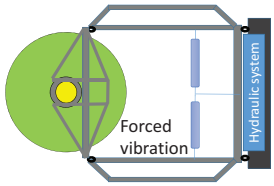

(c) Top view of forced vibration set-up.

Fig. 2: Principle sketch of MARINTEK's full scale VIV test rig.

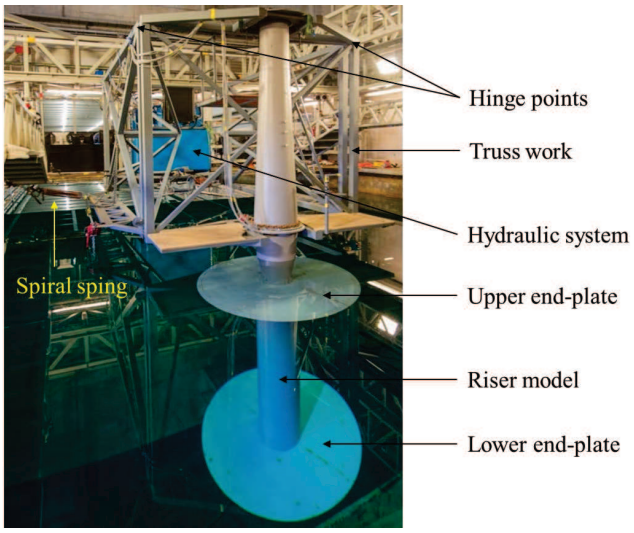

Fig. 3: Photo of the test rig with smooth riser model.

excitation on this part, but since both the length and the diameter are much smaller than the riser model, this effect regarded to be small.

The hinged test rig enables the tested riser model to move in a semi-arc path with a radius of 5 m. When the CF oscillation amplitude is half the diameter (0.267 m), the hinged arm rotates around 3 degrees from the mean position. This rotation angle is small, the resulting IL motion amplitude is about 1.5 cm, about 2.8% of the cylinder diameter. So, we assume present VIV test results can be interpreted as pure CF responses.

A small IL component results in the oscillation orbits shown in Fig. **??**. When we perform the tests, the towing carriage run in both directions along the tank. As illustrated in Fig. **??** and Fig. **??**, the oscillation orbits have the same shape, but the current direction is opposite. The two orbits then have different phase angles, where the difference is 180 degrees.

Marine risers and pipelines usually have VIV with combined CF and IL motions. Pure IL VIV only occurs at reduced velocities lower than the onset of the CF responses. The response amplitude of pure IL VIV is much smaller than IL in combination with CF. The IL component attracts attention because its frequency is usually twice that of the CF frequency, even if IL has a smaller response amplitude, it may accumulate considerable fatigue damage. In practice, if the current is assumed to attack at one direction, pure CF assumption is sufficient.

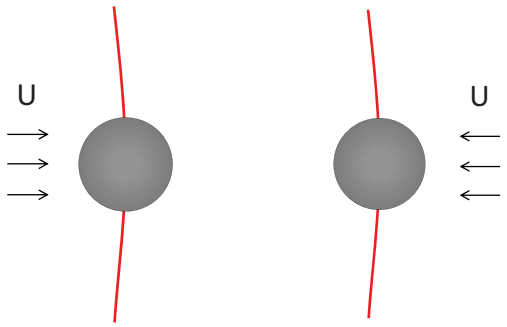

(a) (b)

Fig. 4: Illustration oscillation orbits with different phase angles when the towing directions are opposite.

Table 1: Key properties of the riser model.

Property	**Unit**	**Value**
Length of the riser model, L	m	3.270
Outer diameter, D	m	0.533
Thickness	m	0.002
k/D of smooth riser model	-	5.3×10^{-5}
k/D of rough riser model	-	1.0×10^{-3}

Some tests have been repeated either by towing in the same direction or by towing opposite directions. Some variability of the CF motion was observed. It was not found that the responses are sensitive to towing directions.

For free oscillation VIV tests, the test rig was elastically mounted using tension coil springs to obtain a desired natural period T_n.

In [?], one spring set-up was used for all the free oscillation tests, so the system has the same natural oscillation frequency in water. To achieve different reduced velocities, the towing speed was varied, and thus the Re. In the present tests, the Re was kept the same, and we tuned the natural oscillation period to achieve the desired reduced velocity. Three sets of tension coil springs were deployed and mounted at various positions along the test rig to achieve the natural periods wanted.

Forced motion tests were also conducted in a later phase, in which the spring system was replaced by a hydraulic system. The desired oscillation amplitude and frequency were input to the control system and achieved by the hydraulic cylinders.

The entire system was towed by the carriage through calm water to simulate uniform current past the riser section.

4 Riser Models

Two steel pipes were manufactured to model full-scale riser sections. One was painted to have a smooth outer surface, and the other was wrapped with P36 sandpaper to model a rough outer surface due to marine growth (see Fig. **??**). The key properties of the riser models are shown in Tab. **??**.

The riser model has a length-to-diameter ratio of 6.135. Test results such as drag coefficients, and the response amplitude ratio from [?] agree well with other literature [?], which indicates the riser model is sufficient long enough to avoid 3D flow effects.

5 Instrumentation

The following instrumentation/measurements are included:

1. The standard measuring equipment on the towing carriage measured towing speed.
2. In [?], the forces acting on the test riser model were measured by use of an assembled set of one-component force transducers, which were mounted on the riser model end.

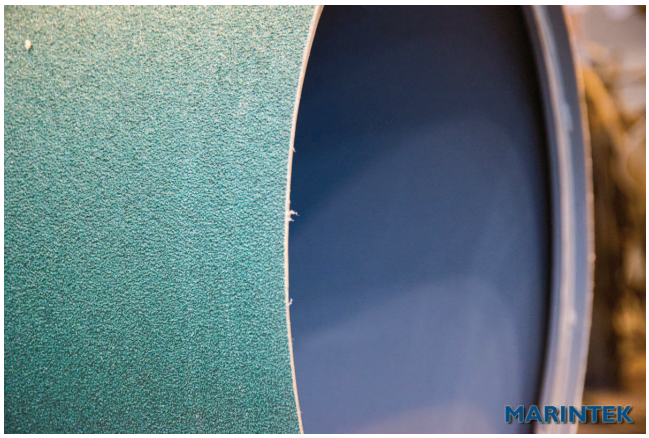

Fig. 5: Rough surface modelled by sandpaper, $k/D = 1.0 \times 10^3$.

In the present model tests, a central core riser was manufactured and equipped with strain gauge force transducers, which measured the bending moments at four stations of the inner core riser, see Fig. **??**.
The tested riser model was fastened to the inner core riser at two connection points in the middle of the riser section. There was no other contact between the riser model and inner core beam. There were also small gaps between the riser model and two end-plates.
The basic principle is to use the difference in bending moments to derive shear force: $F = \Delta M/\Delta l$. By using the measured bending moments at Station 3 and Station 4, the force acting on the lower end-plate F_L was calculated. In the same way, the force acting on the riser model was found F_U. The force acting on the riser model was found as $F_U = F - F_L$.
The inner central core riser is mounted onto the test rig and oscillates together with the riser model. Since the test rig is hinged, the heading of the riser model does not change during one oscillation.

3. The riser oscillation displacement was measured by an optical tracking system (OQUS); in addition, a potentiometer measured the rig oscillations.
4. A three-component accelerometer was located at the topside of the rig on the 'cone-shape' support structure. Measured accelerations were used to document vibrations in the test rig.

All the transducer signals were sampled at 1200 Hz except the OQUS, which has a sampling frequency of 25 Hz. The low-pass analogue filtering cut-off frequency was 250 Hz. The force transducers and accelerometers have measurement accuracy of higher than 98% of measured value for significant response levels. OQUS has dynamic resolution less than 0.5 mm. Calm water conditions for each test run were assured by waiting at least 10 minutes between tests.

6 Test Program

The following tests were carried out:

1. Instrumentation verification and calibration tests.
2. Decay tests and pluck tests in air and still water.
3. Stationary tests.
4. Pure CF free oscillation tests.
5. Pure CF forced oscillation tests

Decay tests were performed in air on the test rig without the riser model, to investigate the structural damping of the test rig. The damping ratio was found to be between 1-2%. Fig. **??** shows the time history of displacement at the riser location of one decay test in air.

Decay tests were also performed in still water for each spring set, before the free oscillation test. The natural frequencies in water and the damping ratio were measured for each decay test in water. Figure **??** shows the time history of displacement at the riser location of one decay test in water. The damping ratio was 3.6%.

Stationary tests were performed on both fixed smooth and rough riser models, at the Re range from subcritical to critical regimes.

Free oscillation tests were performed on both smooth and rough riser models, at selected critical Re and a range of reduced velocities. In addition, some tests in [?] were repeated with varying Re. The test program of stationary and free oscillation tests is shown in Tab. **??**.

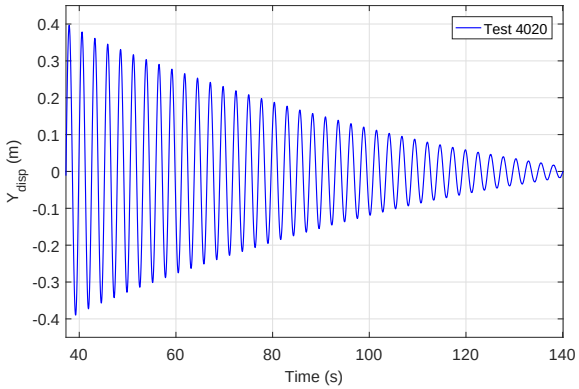

Fig. 6: Decay test in air, without riser model, $T_n = 2.62\ s$, damping ratio is 1.3%.

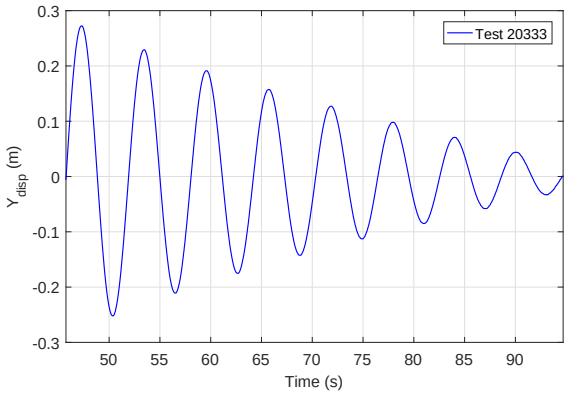

Fig. 7: Decay test in air, without riser model, $T_n = 5.82\ s$, damping ratio is 3.6%.

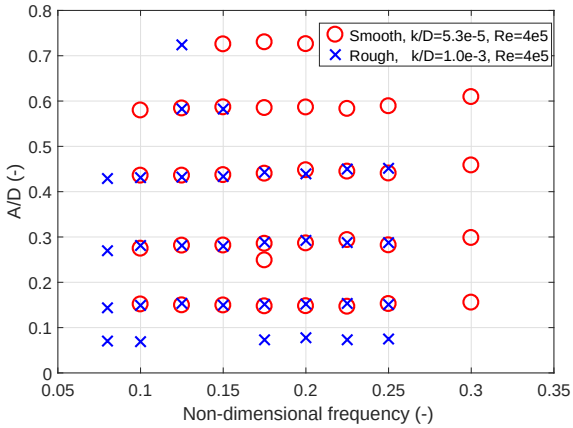

Fig. 8: Test matrix of forced motion tests.

Forced motion tests were carried out at $Re = 4 \times 10^5$, on both smooth and rough riser models. The test matrix with varying amplitude ratios (A/D) and non-dimensional oscillation frequencies ($\hat{f} = f_{osc}D/U$) is presented in Fig. **??**. The purpose of these tests was to establish a prototype Re hydrodynamic force coefficient database which can be further used by VIV analysis programs such as VIVANA [**?**].

Table 2: Test program of stationary and free oscillation tests.

	k/D	**Re**	U_r
Stationary tests	5.3×10^{-5}	9×10^{4} - 8×10^{5}	-
	1.0×10^{-3}	9×10^{4} - 6×10^{5}	-
Free oscillation tests	5.3×10^{-5}	1×10^{5} - 2.6×10^{5}	5 - 12
	5.3×10^{-5}	3×10^{5}	4 - 10
	5.3×10^{-5}	4×10^{5}	5 - 13
	5.3×10^{-5}	6×10^{5}	5 - 11
	1.0×10^{-3}	2.5×10^{5} - 3.5×10^{5}	7 - 11
	1.0×10^{-3}	2×10^{5}	4 - 8
	1.0×10^{-3}	4×10^{5}	8 - 12

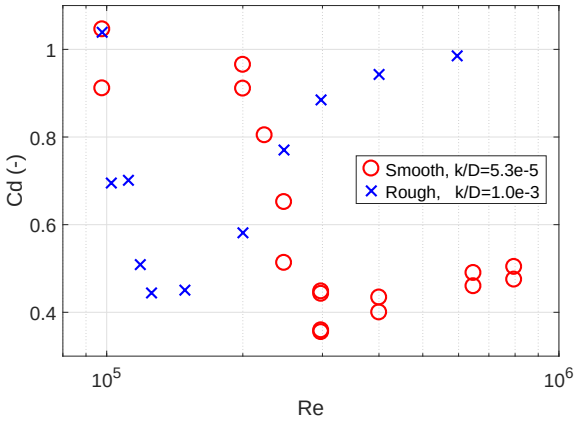

Fig. 9: Drag coefficients from stationary tests.

7 Results

7.1 Drag coefficient

Drag coefficients of both smooth and rough circular cylinders are presented in Fig. **??** as results from the stationary tests. The effects of the surface roughness ratio on the drag coefficient is clearly seen. 'Drag crisis' is a phenomenon in which the drag coefficient decreases abruptly as the Reynolds number increases. Simultaneously, the boundary layer flow around the bluff body transits from laminar to turbulent [**?**]. The rough cylinder has 'drag crisis' at $Re = 1.26\times10^{5}$, while the smooth cylinder has the 'drag crisis' at $Re = 2.98\times10^{5}$. The lowest drag coefficient of the rough cylinder (0.44) is larger than that of the smooth cylinder (0.36). This is consistent with existing literature [?]. Due to roughness at the cylinder surface, the transition of the boundary layer from laminar to turbulent occurs at lower Reynolds numbers. Consequently, the critical and supercritical flow regimes shift to lower Reynolds numbers [**?**]. When the surface roughness ratio is larger than a critical value, the 'drag crisis' disappears accordingly [**?**] [**?**].

7.2 Strouhal number

Spectral analysis has been performed on the CF force of stationary tests. The peak frequencies correspond to the vortex shedding frequency f_v. It is important to note that this is the vortex shedding frequency from a stationary cylinder. It is well known that the Strouhal number is defined as $St = f_v D/U$, the calculated Strouhal number is shown in Fig. **??**.

Figure **??** shows that when Re is in the range 9×10^{4} - 8×10^{5}, the St of both cylinders is between 0.15 and 0.25. The St at Re from 3×10^{5} to 8×10^{5} is slightly lower than the St at Re from 1×10^{5} - 3×10^{5}. The rough cylinder ($k/D = 1.0\times10^{-3}$) has relative higher St than the smooth cylinder. These observations agree well with existing data and findings [?].

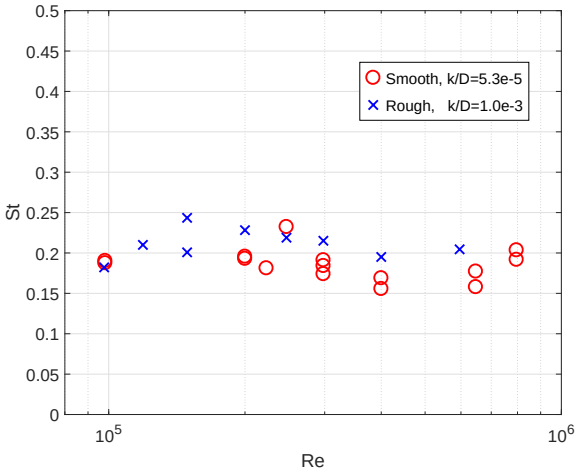

Fig. 10: Strouhal number from stationary tests.

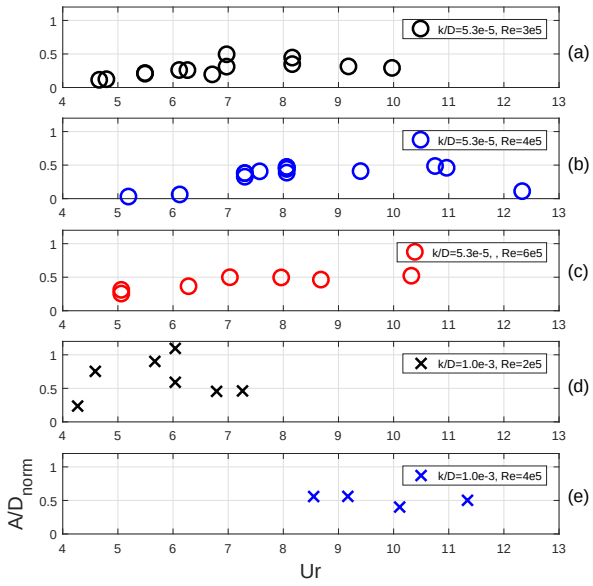

Fig. 11: A_{nom}/D vs. U_r at prototype Re.

7.3 Response amplitude ratio

The Reynolds effect on the maximum VIV response amplitude ratio was discussed in [?], where distinct Re effects between subcritical, critical and supercritical Re flow regimes were observed.

Nominal CF VIV amplitude ratios ($A_{nom}/D = \sqrt{2}\sigma_{CF}/D$) of the present tests are shown in Fig. **??**, plotting against the reduced velocity at different Re.

Free oscillation tests on the smooth riser ($k/D = 5.3\times10^{-5}$) were performed at three Reynolds numbers: 3×10^5, 4×10^5 and 6×10^5. Among these three sets of free oscillation tests, Re was kept the same for each set by towing the carriage at the same speed. Different reduced velocities were achieved by changing the spring set-up. These three Reynolds numbers are within the 'critical' and 'supercritical' flow regimes. It shows that the maximum A_{nom}/D is around 0.5 for all three Re numbers. It implies that for a smooth riser, in critical and supercritical flow regimes, the maximum response amplitude is not sensitive to Re.

Free oscillation tests on the rough riser ($k/D = 1.0\times10^{-3}$) were performed at two Reynolds numbers: 2×10^5 and 4×10^5. At $Re = 2\times10^5$ (subcritical flow regime), maximum A_{nom}/D is around 1.1, the corresponding U_r is around 6. At $Re = 4\times10^5$ (critical flow regime), maximum A_{nom}/D is around 0.56, the corresponding U_r is 8.55 and 9.17. The effect of Re on the maximum response amplitude ratio is significant and the trend is very similar for both smooth and rough risers. Further

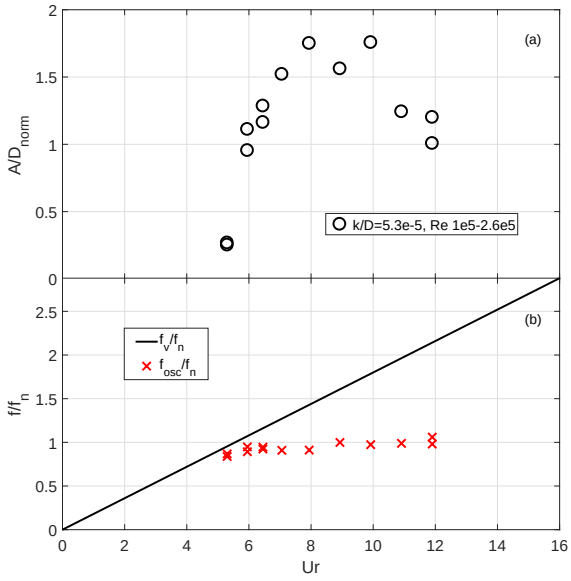

Fig. 12: Smooth cylinder CF VIV response at subcritical Re. (a) A_{nom}/D vs. U_r. (b) Oscillation frequency to still water natural frequency ratio.

Table 3: Maximum amplitude ratio.

Re	$A_{nom,max}/D$	
	$\frac{k}{D} = 5.3 \times 10^{-5}$	$\frac{k}{D} = 1.0 \times 10^{-3}$
1×10^5 - 2.6×10^5	1.76	-
2×10^5	-	1.1
3×10^5	0.49	-
4×10^5	0.48	0.56
6×10^5	0.49	-

discussion will confirm this.

If we compare the results at the same Re 4×10^5 for both smooth and rough risers, the maximum A_{nom}/D values are 0.5 and 0.56 respectively, which implies that the effect from the surface roughness is not significant at this Reynolds number. Earlier studies also showed that the roughness has limited influence on the VIV response in the subcritical Re range [?]. However, no tests with the rough cylinder were carried out in the subcritical Re range in the present test.

One set of free oscillation tests on the smooth riser was carried out by using the same spring set-up, but towing the carriage with different speeds, in such a way that both the Re and reduced velocity would be different from test to test. The results are shown in Fig. **??**a. Note that the Re varies from 1×10^5 and 2.6×10^5, which is mainly in the subcritical flow regime. We can see that the maximum A_{nom}/D is around 1.76, which is significantly higher than the prototype Re number results. A similar high maximum amplitude ratio was also observed in the previous prototype Re VIV tests [?]. The results from both previous and present tests show that the smooth riser has a much higher amplitude in the subcritical flow regime than in the critical and supercritical flow regime. In the subcritical flow regime, the maximum response amplitude ratio measured by using present full-scale VIV test rig agrees with results from existing literature [?] [**?**] in general.

In Fig. **??**b, the ratio between oscillation frequency and still water natural frequency is compared with the ratio between the Strouhal frequency and still water frequency. It is clearly seen that the oscillation frequency is synchronized with the natural frequency in the reduced velocity range from 6 to 12, which is called lock-in. It also shows that f_{osc}/f_n is around 1.0, which indicates the added mass is close to the added mass in still water.

The maximum amplitude ratios in the CF direction are summarized in Tab. **??**, for both smooth and rough riser models.

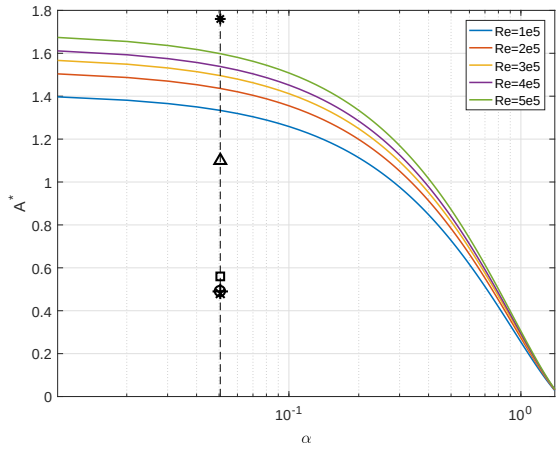

$*$, $Re = 2.16 \times 10^5$, $k/D = 5.3 \times 10^{-5}$
$\bigcirc$, $Re = 3 \times 10^5$, $k/D = 5.3 \times 10^{-5}$
$\times$, $Re = 4 \times 10^5$, $k/D = 5.3 \times 10^{-5}$
$+$, $Re = 6 \times 10^5$, $k/D = 5.3 \times 10^{-5}$
$\triangle$, $Re = 2 \times 10^5$, $k/D = 1.0 \times 10^{-3}$
$\square$, $Re = 4 \times 10^5$, $k/D = 1.0 \times 10^{-3}$

Fig. 13: Calculated peak response amplitude ratio by 'Modified Griffin Plot' [?].

Govardhan & Williamson [?] proposed an empirical formula for peak CF response amplitude ratio:

$$A^* = (1 - 1.12 + 0.30\alpha^2) log(0.41 Re^{0.36}) \tag{12}$$

where α is a mass-damping parameter, $\alpha = (m^* + C_a)\zeta$. C_a is the potential added mass coefficient, taken as 1.0 for a circular cylinder.

Although this formula is only valid for a range of Re=500 - 33000 [?], an attempt has been made to show the differences of Re effect on the peak response amplitude ratio in subcritical and prototype Re. Here we take $\zeta = 0.036$ from Fig. **??**, which gives $\alpha = 0.0506$.

The maximum response amplitude ratios in Tab. **??** are plotted together with the 'Modified Griffin Plot' (defined by formula (**??**), see Fig. **??**.

It is expected that the results from present experiments do not agree with the 'Modified Griffin plot', because the Re is out of the valid range of formula (**??**). But if we take a closer look, at Re around 2×10^5, the smooth pipe has $A^* = 1.76$, while the rough pipe has $A^* = 1.1$. It is reasonable to believe that the difference is caused by the surface roughness. This Reynolds number is in the TrS0 regime, where the shear layer is fully turbulent, and there is onset of transition from laminar to turbulent at separation point [**?**]. Larger surface roughness makes this transition occur at a lower Re.

Fluctuating lift and drag coefficients were reviewed and presented in Fig. **??** by [?]. In the TrS0 regime, the lift coefficient decreases dramatically, and this has a direct effect on the A^*. The relationship between A^* and the lift coefficient is described in [**?**]:

$$A^* = \frac{C_L}{\frac{8m\zeta\pi^2 St^2}{\rho D^2}} \tag{13}$$

where we can see that under lock-in condition (vortex shedding frequency synchronizes with the cylinder natural frequency), A^* is independent of the flow velocity (Re), but directly influenced by the lift coefficient. What happens if we have a larger surface roughness? As we discussed earlier, it makes this transition occur at lower Re. In other words, at the same Re, the lift coefficient for a rougher cylinder is smaller than that of a smooth cylinder, especially at TrS0 regime. That explains the difference of A^* between a smooth and a rough cylinder.

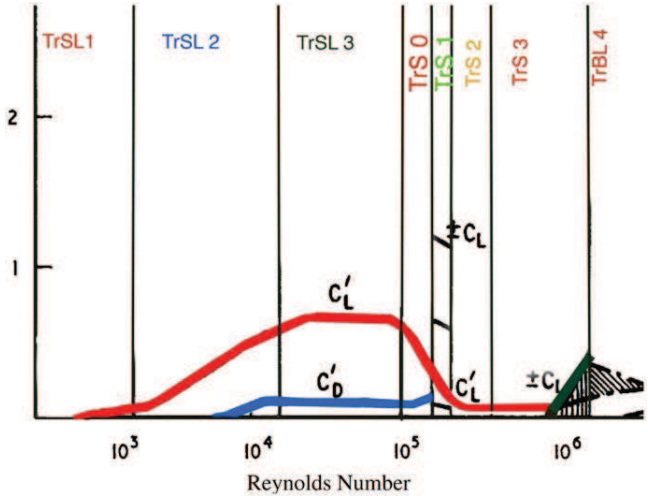

Fig. 14: Fluctuating lift (C'_L) and drag (C'_D) coefficients, and mean lift (C_L) coefficient the Transition in shear layer (TrSL), Transition around separation (TrS) and Transition in boundary layer (TrBL) regimes [?] [?].

For the three data points with A^* in the range of 0.4 to 0.6, it seems they are neither Re dependent nor sensitive to surface roughness. They have a Re range from 3×10^5 to 6×10^5, corresponding approximately to the TrS1 to TrS3 regimes. In these regimes, the boundary layer transits from laminar to turbulent, and the shear layer is fully turbulent; the surface roughness plays a less important role. The lift coefficient is significantly low and varies little with further increasing Re, so that the A^* is also less sensitive to Re.

7.4 Oscillation frequency

In free oscillation VIV tests, if the vortices shed at a frequency that is close to the natural frequency of test apparatus, the two frequencies tend to synchronize with each other, a phenomenon called lock-in. Under the lock-in condition, the vortex shedding frequency no longer follows the Strouhal relation ($St = f_v D/U$). Instead, the vortex shedding frequency equals the oscillating frequency. Lock-in occurs at a certain range of reduced velocity, which depends on the structural damping and mass ratio. Low mass ratio structures such as marine risers may have lock-in with a wider range of reduced velocity.

Fig. **??** plots the dominant oscillation frequency against the natural frequency in still water (measured from decay tests in water). It illustrates the difference between added mass in still water and in constant current. The scattering is seen. For a mass-damper-spring system, assuming the damping is small enough to be ignored, $f = \sqrt{k/(m+m_a)}$, the frequency ratio is

$$\frac{f_{osc}}{f_n} = \sqrt{\frac{m+m_{a,n}}{m+m_{a,osc}}} = \sqrt{1+\frac{m_{a,n}-m_{a,osc}}{m+m_{a,osc}}} \tag{14}$$

where $m_{a,n}$ is the added mass in still water, $m_{a,osc}$ is the added mass when the riser model is freely oscillating.

For the smooth riser model, $f_{osc}/f_n < 1$ at $Re = 3\times10^5$, which indicates that the oscillating added mass is larger than the still water added mass. At $Re = 4\times10^5$, $f_{osc}/f_n > 1$ for most of the cases of smooth riser model, this is true also for the rough riser model, indicating that the oscillating added mass is smaller than the still water added mass.

7.5 Transition

'Transition' could happen for the elastically supported riser model in constant flow [**?**], this has also been observed in the present tests. Under the same towing speed, the transition of the wake-induced force will result in different responses, as shown in Fig. **??**.

Distinct different response amplitudes are observed in two time windows, where the oscillation periods are slightly different. The 'transition' occurred at $t = 250\ s$, the lift force is in phase with the oscillation displacement all the time.

7.6 Excitation coefficient

The excitation coefficients obtained from the forced motion tests are presented as contour plots in Fig. **??** and Fig. **??**. All the forced motion tests were carried out at the same Reynolds number, 4×10^5. Note that in the contour plots, the values of the area without data points are interpolated.

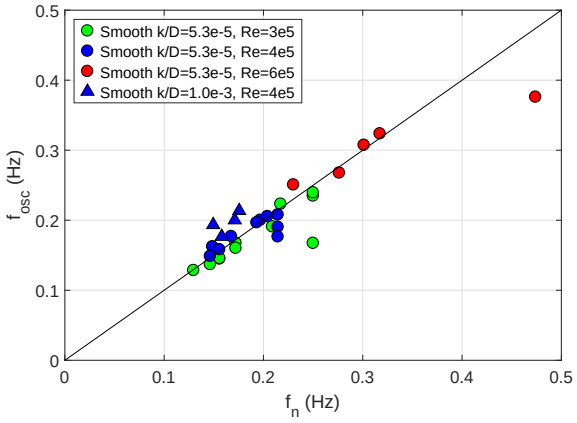

Fig. 15: Oscillation frequency vs. still water natural frequency.

Table 4: Comparison of excitation coefficients for rough riser.

Property	**Present rough riser**	**ExxonMobil [?]**
k/D	1.0×10^{-3}	2.0×10^{-3}
Excitation region	$\hat{f}$: 0.11 - 0.195	U_r: 2.5 - 9.5
$A_{CF,max}\|_{C_e=0}/D$	0.65	0.85
$C_{e,CF,max}$	$\geqslant 0.3$	$\geqslant 0.5$

In the contour plots, the zero contour lines define the CF response amplitude for a cylinder without mechanical damping. The areas with positive excitation coefficients are defined as excitation regions, and the zero-contour line is the boundary of these regions [?].

From the contour plot of the smooth riser, two excitation regions are clearly seen: one is with $\hat{f}$ from 0.1 to 0.15, while the other is with $\hat{f}$ from 0.275 to 0.3. It also indicates that the excitation region may extend to the non-dimensional frequency lower than 0.1 and higher than 0.3. The maximum amplitude ratio corresponding to zero excitation coefficient is slightly higher than 0.6. This value may change if additional data points are available.

For the riser section with a rough surface, calculated excitation coefficients from forced oscillation tests are presented in Fig. **??**. Positive excitation coefficients for the rough riser section are seen at non-dimensional frequencies 0.125, 0.15 and 0.175. The maximum excitation coefficient is around 0.3 at $\hat{f} = 0.175$. The non-dimensional frequency ranges from 0.11 to 0.19 in the excitation region. The maximum amplitude ratio with zero excitation coefficient is around 0.65. For the $\hat{f}$ larger than 0.25, it is unknown whether there exists another excitation region. For the $\hat{f}$ lower than 0.09, there exists a tiny excitation region, with very high uncertainty due to the lack of data points. In the present model tests, the rough riser model has a surface roughness ratio $k/D = 1.0\times10^{-3}$, which is half of one model of [?], so the results should be comparable. The comparison is summarized in Tab. **??**. In general, results from the present study have a similar trend and the excitation coefficients have the same level of magnitude.

From Fig. **??** and Fig. **??**, we can see that the number of data points is limited, values in large areas of the contour plots are interpolated. Contour plots with higher resolution and more accurate excitation coefficients are expected if more tests are carried out. Especially in the excitation regions, higher excitation coefficient may appear if additional tests are performed.

The differences between the present tests and [?] may be attributed to several aspects:

1. The present test has a fixed Re, while ExxonMobil has a varying Re.
2. The surface roughness ratio is not the same between the present and the ExxonMobil tests.
3. The present full scale riser model was located vertically on the test rig, while ExxonMobil had a horizontal cylinder model.
4. The excitation forces were extracted in different ways.
5. The L/D is around 6 in present tests, ExxonMobil has L/D of 18.

Validation of the excitation coefficients at prototype Re is difficult. One is to compare with results in other literature

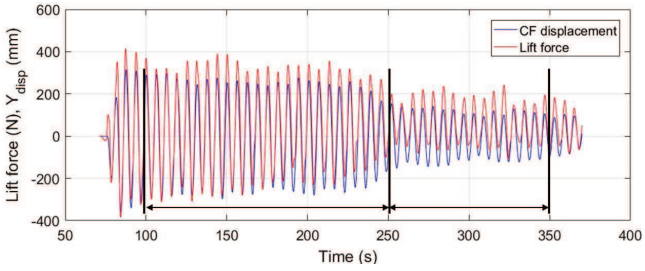

(a) Time histories of lift force and CF displacement

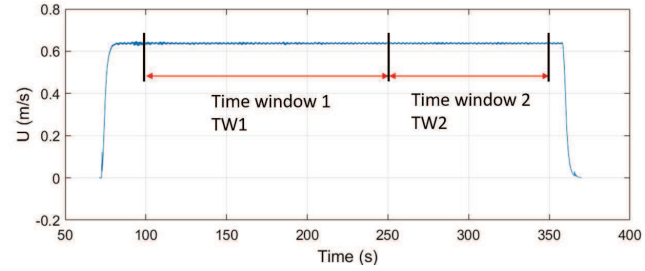

(b) Time histories of towing speed and selection of two time-windows.

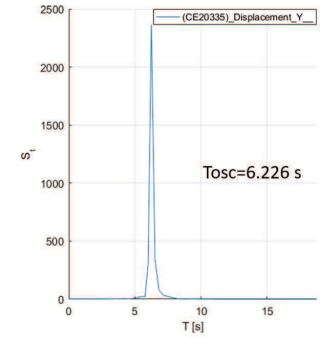

(c) PSD of Y_{disp} in TW1.

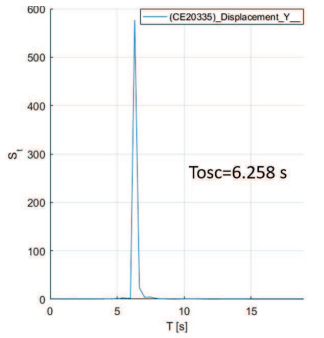

(d) PSD of Y_{disp} in TW2.

Fig. 16: Free oscillation test on the smooth riser, $k/D = 5.3 \times 10^{-5}$, $Re = 3 \times 10^5$, $U_r = 7$.

such as [?], see Tab. **??**. Unfortunately, there are limited amount of relevant published results. Another way is to apply these coefficients to predict the VIV responses of a realistic case, and compare with measured responses. For example, field response measurement of a real marine riser. However, due to lack of such available data, this has not been done.

Another point in the validation process is to check if the amplitude ratio A_{nom}/D found from free oscillation tests agrees with the forced oscillation tests when the excitation coefficients are zero. In present study, it is found that the amplitude ratios are consistent between free and forced oscillation tests.

The drag coefficients of all the forced motion VIV tests are plotted against the amplitude ratio, which is shown in Fig. **??**. Note that the amplitude ratio is the actual measured value instead of the defined value. For the smooth riser, the drag coefficient varies from 0.4 to 1.1. For the rough riser, the drag coefficient ranges between 0.85 and 1.3, which is significantly larger than for the smooth riser. At this Reynolds number the fixed smooth riser model has a drag coefficient of around 0.4, and the fixed rough riser model has a drag coefficient of about 0.95, see Fig. **??**. The drag amplification due to CF motion is seen, as the amplitude increases, this amplification becomes stronger. In general, scattering of the drag coefficients of rough riser tests is larger than for smooth riser tests. Since the rough riser has a larger stationary drag coefficient at this Re, under the same amplification factors, larger scattering will be seen, as shown in Fig. **??**.

Scattering of the drag coefficients is seen at the same amplitude ratio. For each group of scattered results, the oscillating amplitudes and towing speeds are the same, but with different oscillation frequencies f_{osc}. One possible reason for this scattering is the variation in oscillation frequency. It is reasonable to believe that under the same forced oscillation amplitude, the test with lower oscillation frequency may have a lower drag coefficient compared to the test with higher oscillation frequency, see Fig. **??**. Imagining a test with extremely small oscillation frequency, the model can be considered quasi-stationary. In such case, the drag coefficient is not amplified much, and vice versa. The trend of C_d versus $\hat{f}$ and A/D is found to be similar results from forced oscillation tests in [**?**].

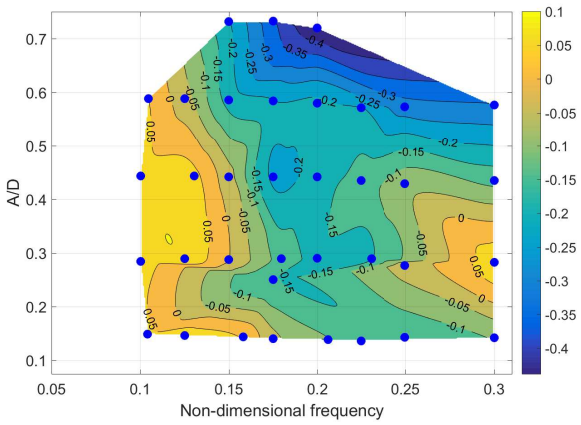

Fig. 17: Plot of contour curves for CF excitation coefficient in an amplitude ratio - non-dimensional frequency map, $k/D = 5.3 \times 10^{-5}$, $Re = 4 \times 10^5$. Data points are marked with blue dots.

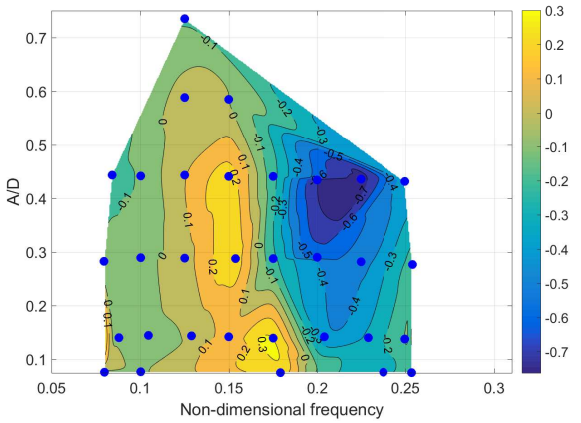

Fig. 18: Plot of contour curves for CF excitation coefficient in an amplitude ratio - non-dimensional frequency map, $k/D = 1.0 \times 10^{-3}$, $Re = 4 \times 10^5$. Data points are marked with blue dots.

8 Conclusions

This paper presents some key results of the prototype Re VIV model tests that have been carried out at MARINTEK. Stationary towing tests, free oscillation VIV tests and forced motion VIV tests on the two full-scale rigid riser sections were conducted.

Drag coefficients of 'fixed' riser sections are extracted from stationary tests. The surface roughness effect on the drag coefficient is clearly seen, and the drag crisis is captured for both riser sections. It might be of interest to do more stationary tests with even higher Reynolds numbers and different surface roughness ratios to get a more complete data base.

Pure CF free oscillation VIV tests in the present study were carried out at fixed Reynolds numbers, different reduced velocities were achieved by adjusting the location and arm length of three sets of springs. The key results are the response amplitude ratio. For either the smooth or the rough riser model in the present study, in critical and supercritical flow regimes, the displacement amplitude ratio is not sensitive to Re. However, in the subcritical flow regime, the response amplitude ratio is significantly larger than that in critical and supercritical flow regimes for the smooth cylinder. At a supercritical Reynolds number 4×10^5, the maximum displacement amplitude ratio is found to be sensitive to the surface roughness.

Forced oscillation VIV tests were carried out on both riser section models at a Reynolds number 4×10^5. The most important results are the excitation coefficients at the prototype Reynolds number. Two excitation regions for the 'smooth riser' and one excitation region for the 'rough riser' are identified.

The excitation coefficient at supercritical Re in the present study is significantly lower than the excitation coefficients in subcritical flow. Partly due to insufficient data. The excitation region is also different, especially for the riser with a rough surface. Amplified drag coefficients are also extracted from forced oscillation VIV tests. Generally, results from the present study show similar trends to the literatures.

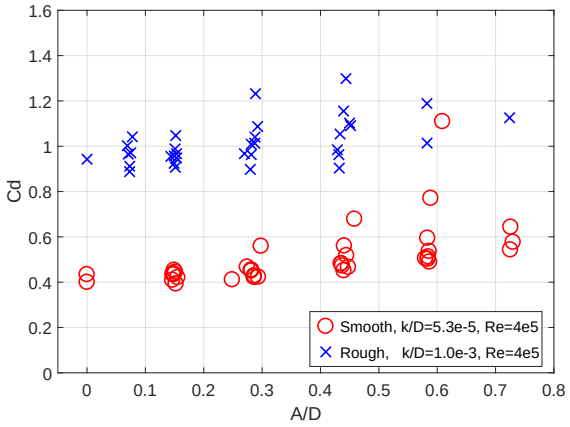

Fig. 19: Drag coefficients of all forced motion VIV tests.

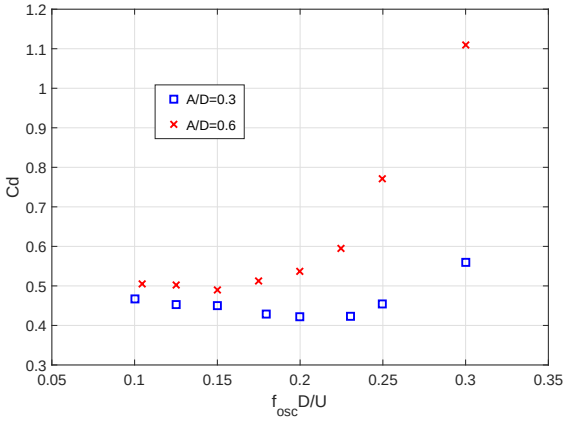

Fig. 20: Drag coefficients of two series of forced oscillation tests of smooth riser, $k/D = 5.3 \times 10^{-5}$, $Re = 4 \times 10^5$.

Acknowledgements

The authors are grateful to the Norwegian Deepwater Programme and STATOIL for permission to publish these results.

References

[1] Yin, D., Wu, J., Lie, H., Baarholm, R., and Larsen, C. M., 2015. "VIV prediction of steel catenary riser - A Reynolds number sensitivity study". In Proceedings of the Twenty-fifth (2015) International Ocean and Polar Engineering Conference, Vol. 3, pp. 1018–1027.

[2] Klamo, J., Leonard, A., and Roshko, A., 2005. "On the maximum amplitude for a freely vibrating cylinder in cross-flow". *Journal of Fluids and Structures,* **21**(4), pp. 429–434.

[3] Govardhan, R. N., and Williamson, C. H. K., 2006. "Defining the modified griffin plot in vortex-induced vibration: revealing the effect of reynolds number using controlled damping". *Journal of Fluid Mechanics,* **561**, pp. 147–180.

[4] Swithenbank, S. B., Vandiver, J. K., Larsen, C. M., and Lie, H., 2008. "Reynolds number dependence of flexible cylinder VIV response data". In Proceedings of the 27th International Conference on Offshore Mechanics and Arctic Engineering, no. OMAE2008-57045.

[5] Resvanis, T. L., Vandiver, J. K., and Liapis, S., 2012. "Reynolds number effects on the vortex-induced vibration of flexible marine risers". In Proceedings of the 31th International Conference on Offshore Mechanics and Arctic Engineering, no. OMAE2012-83565.

[6] Ding, Z. J., Balasubramanian, S., Lokken, R. T., and Yung, T.-W., 2004. "Lift and damping characteristics of bare and straked cylinders at riser scale Reynolds numbers". In Offshore Technology Conference, no. OTC-16341.

[7] Dahl, J. M., Hover, F. S., Triantafyllou, M. S., and Oakley, O. H., 2010. "Dual resonance in vortex-induced vibrations at subcritical and supercritical reynolds numbers". *Journal of Fluid Mechanics,* **643**, pp. 395–424.

[8] Lie, H., Szwalek, J. L., Russo, M., Braaten, H., and Baarholm, R. J., 2013. "Drilling riser VIV tests with prototype

Reynolds numbers". In Proceedings of the ASME 32nd International Conference on Ocean, Offshore and Arctic Engineering, no. OMAE2013-11643.

[9] Yin, D., Lie, H., and Baarholm, R. J., 2017. "Prototype Reynolds number VIV tests on a full-scale rigid riser". In Proceedings of the ASME 37th International Conference on Ocean, Offshore and Arctic Engineering, no. OMAE2017-61415.

[10] Aronsen, K. H., 2007. "An Experimental Investigation of In-line and Combined In-line and Cross-flow Vortex Induced Vibrations". PhD thesis, Norwegian University of Science and Technology, Trondheim, Norway.

[11] Yin, D., 2013. "Experimental and Numerical Analysis of Combined In-line and Cross-flow Vertex Induced Vibrations". PhD thesis, Department of Marine Technology, Norwegian University of Science and Technology, Trondheim, Norway.

[12] Passano, E., Larsen, C. M., Lie, H., and Wu, J., 2015. VIVANA Theory Manual Release 4.6 rev.0. Tech. Rep. MT2014 F-135, MARINTEK.

[13] Newman, J. N., 1999. *Marine Hydrodynamics*. The MIT Press.

[14] Bridge, C., Willis, N., Sworn, A., and de Wilde, J., 2005. "Development of SHEAR 7 Lift Curves For VIV Analysis And Application To Single Pipe And Bundle Risers". In Offshore Technology Conference.

[15] Miller, B., 1976. *The Hydrodynamic Drag of Roughened Circular Cylinders*. NMI R. National Maritime Institute (Feltham).

[16] Hoerner, S. F., 1965. *Fuild-Dynamic Drag*. Hoerner Fluid Dynamics, Bakersfield, CA, USA.

[17] Raghavan, K., and Bernitsas, M. M., 2011. "Experimental investigation of Reynolds number effect on vortex induced vibartion of rigid circular cylinder on elasstic supports". *Ocean Engineering,* **38**, pp. 719–731.

[18] Zdravkovich, M. M., 2002. *Flow Around Circular Cylinders, Vol 1: Fundamentals*. Oxford University Press.

[19] Blevins, R. D., 1990. *Flow-Induced Vibration*, 2 edition ed. Krieger Publishing Company, Kriegerdrive, Florida, USA.

[20] Carberry, J., Sheridan, J., and Rockwell, D., 2005. "Controlled oscillations of a cylinder: forces and wake modes". *Journal of Fluid Mechanics,* **538**, pp. 31–69.

[21] Gopalkrishnan, R., 1993. "Vortex Induced Forces on Oscillating Bluff Cylinders". PhD thesis, MIT, Dep. of Ocean Engineering, Cambridge, MA, USA.